Precursory deformation and fracture before brittle rock failure and potential application to volcanic unrest

Christopher Kilburn[1]

Received 23 July 2011; revised 19 December 2011; accepted 21 December 2011; published 24 February 2012.

[1] Small-magnitude earthquakes and ground deformation are the precursors most frequently recorded before volcanic eruptions. Analogous signals (using acoustic emissions) have also been reported before the bulk brittle failure of crustal rock in the laboratory. Models based on laboratory and field data have focused on precursory behavior during deformation under a constant stress. A new model is proposed for extending analyses to deformation under an increasing stress. It describes how precursory time series can be determined from a parent relation between fracturing and stress, together with time-dependent changes in applied stress and rock resistance. The model applies to rock in which these stresses do not interact with each other and occupy volumes much smaller than the total volume being deformed. It identifies how the amounts of fracturing observed during deformation are controlled not only by stress concentrations at macroscopic heterogeneities, such as crack tips but also by rock composition, temperature, confining pressure, and the distribution of energy among atoms. The results appear to be scale independent, and so may be used to investigate whether the approach to bulk failure is limited by changes in applied stress or in rock weakening. When applied to pre-eruptive data from Hawaii, the analysis suggests that precursory signals are controlled by an increase in applied stress, rather than by creep deformation under a constant stress.

Citation: Kilburn, C. (2012), Precursory deformation and fracture before brittle rock failure and potential application to volcanic unrest, *J. Geophys. Res.*, *117*, B02211, doi:10.1029/2011JB008703.

1. Introduction

[2] Volcanic eruptions are commonly preceded by increasing rates of ground deformation and of local fracturing of the crust and volcanic edifice [*Voight*, 1988; *McNutt*, 1996; *De la Cruz-Reyna and Reyes-Davila*, 2001; *Kilburn*, 2003; *Zobin*, 2003; *Roman and Cashman*, 2006; *Scandone and Giacomelli*, 2008; *Smith and Kilburn*, 2010; *Bell and Kilburn*, 2011]. Ground deformation records the total strain, caused by distorting atomic bonds in intact rock (modeled as elastic deformation) and by inducing movements along discontinuities during local earthquakes, or volcanotectonic (VT) events (modeled as brittle deformation). VT events, in turn, record the amount of rock damage, which increases until a discontinuity can extend across the volume of crust being deformed. Subsequent movement of the throughgoing discontinuity is then associated with the eruption of ascending magma.

[3] A prevailing strategy for forecasting eruptions has been to quantify repeatable patterns in the contribution of brittle movements to total deformation. Previous studies have been based on empirical analyses of creep deformation, under constant load, as typified by the Voight relation for material failure [*Voight*, 1988, 1989; *Cornelius and Scott*, 1993]. A similar approach has been applied to investigating accelerations in ground movement before slope failure [*Saito*, 1968; *Fukuzono*, 1985; *Voight*, 1988; *Kilburn and Petley*, 2003]. Although creep deformation seems intuitively appropriate before slope failure, it is not evidently the dominant condition before volcanic eruptions, which appear to deform more commonly under an increase in magmatic pressure [*Dzurisin*, 2007].

[4] Here laboratory data on rock fracturing are reanalyzed to propose a new physical model of brittle precursors to bulk failure and to extend studies to deformation under increasing stress. The results show that brittle deformation is controlled by a combination of the macroscopic distribution of applied stress, which determines the preferred locations of fracturing, and the distribution of supplied energy at the atomic level, which determines the probability that fracturing will occur. The results also show how loading conditions determine the patterns of contemporaneous time series for the number of fracture events and for deformation. This result is illustrated by a preliminary application to data from Kilauea, Hawaii, for which precursory signals appear to be controlled by an increase in applied stress, rather than by creep deformation under a constant stress.

2. Empirical Analyses

2.1. Trends From Laboratory Experiments

[5] Studies of the approach to bulk failure have focused on how parameters related to deformation and fracturing vary

[1]Aon Benfield UCL Hazard Centre, Department of Earth Sciences, University College London, London, UK.

0148-0227/12/2011JB008703

with time [*Scholz*, 2002; *Mogi*, 2007]. In the laboratory, localized cracking in rock is recorded using acoustic emissions (AEs), which are triggered by the formation and movement of discontinuities much smaller than the ~1–10 cm dimensions of a sample. Since the pioneering experiments of the 1960s [*Mogi*, 1962; *Scholz*, 1968], published AE studies for crustal rock have been concerned primarily with deformation in compression, normally under a constant load or an increasing load at a constant strain rate, and have confirmed the ubiquitous occurrence of AE before bulk failure at room temperature and confining pressures of as much as 200 MPa (depths of about 8 km), under dry and water-saturated conditions [*Scholz*, 1968; *Hallbauer et al.*, 1973; *Lockner et al.*, 1991; *Lockner*, 1995; *Meredith et al.*, 1990; *Zang et al.*, 1998; *Lei et al.*, 2004; *Benson et al.*, 2007; *Mogi*, 2007], and in simulated volcanic environments to temperatures of at least 600°C [*Rocchi et al.*, 2004; *Burlini et al.*, 2007; *Tuffen et al.*, 2008; *Smith et al.*, 2009].

[6] The time-dependent behavior of fracturing and strain in experiments resembles that recorded in the field [*Fukuzono*, 1985; *Voight*, 1988] and strongly suggests that analogous processes operate over the corresponding range of length scales. Indeed, analyses of multiscale data have produced numerous empirical expressions for describing fracturing and deformation before bulk failure, including Charles' law for the subcritical growth of cracks [*Charles and Hillig*, 1962], the Saito-Fukuzono relation for ground movement before slope failure [*Saito*, 1968; *Fukuzono*, 1985], and Voight's relation for geophysical precursors to volcanic eruptions [*Voight*, 1988].

[7] Although derived from different data sets, the empirical expressions are alternative descriptions of the same underlying trends [*Voight*, 1988, 1989; *Main*, 1999] and can be illustrated by the Voight relation for accelerating creep before bulk failure, in which the acceleration and rate of change of a recorded parameter Ω are related as follows [*Voight*, 1988, 1989]:

$$d^2\Omega/dt^2 = A(d\Omega/dt)^{\alpha} \quad (1)$$

where t is time, A is a constant, and the exponent α lies between 1 and 2. For deformation under constant stress, *Voight* [1988] proposed that the strain, number of fracturing events, and square root of seismic energy release (also called the Benioff strain) can vary in proportion to each other, so that Ω may be used to describe any of these parameters.

[8] Integration of equation (1) shows that rate of change of Ω with time increases exponentially when $\alpha = 1$, but with a power law function of time when $\alpha > 1$ [*Voight*, 1988]. Thus, for $\alpha = 1$,

$$d\Omega/dt = (d\Omega/dt)_0 \exp A(t - t_0) \quad (2)$$

and for $\alpha > 1$,

$$d\Omega/dt = \left[(d\Omega/dt)_0^{-(\alpha-1)} - A(\alpha - 1)(t - t_0)\right]^{-1/(\alpha-1)} \quad (3)$$

where $(d\Omega/dt)_0$ denotes the rate of change of Ω at time t_0. In equations (2) and (3), the parameters A and α determine how $d\Omega/dt$ changes with time, whereas $(d\Omega/dt)_0$ primarily determines the magnitude of $d\Omega/dt$. After rearrangement, equation (3) can be written in terms of the time of failure (t_f) as $d\Omega/dt = (d\Omega/dt)_0\ [1 - (t/t_f)]^{-1/(\alpha-1)}$. The rearranged expression is consistent with damage mechanics models [*Main*, 2000; *Turcotte et al.*, 2003], further supporting the view that equations (1)–(3) describe changes in rock damage before bulk failure.

[9] When Voight's model was first applied to investigate the approach to volcanic eruptions, α was assumed to remain constant throughout a given precursory sequence [*Voight*, 1988; *Voight and Cornelius*, 1991; *Cornelius and Scott*, 1993; *Main*, 1999]. Sequence-averaged values of α were typically found to be greater than 1 [*Voight*, 1988; *Voight and Cornelius*, 1991; *Cornelius and Scott*, 1993] and, as a result, precursory trends have tended to be analyzed preferentially in terms of power law functions of time [*Main*, 1999].

[10] More recent studies of eruption precursors have relaxed the assumption of a constant value for α and, following the analysis of dome extrusions at Mount St. Helens by *McGuire and Kilburn* [1997], have argued that α can evolve from 1 to 2 as fracturing proceeds [*Kilburn and Voight*, 1998; *Kilburn*, 2003; *Smith et al.*, 2009; *Bell and Kilburn*, 2011]. Qualitatively, the evolution has been attributed to rates of VT seismicity being controlled initially by the rate of increase in the number of activated faults (to yield an exponential increase in the rate of precursory signal with time) and later, by the accelerating rate of movement among a preferred number of activated faults (to yield a power law function in the rate of precursory signal with time) [*Kilburn and Voight*, 1998; *Kilburn*, 2003]. Similar behavior has also been observed in rates of cracking before the bulk failure of rock in the laboratory (see section 2.2). Apparently, therefore, the popular power law models of precursors [*Main*, 1999, 2000; *Kilburn*, 2003; *Turcotte et al.*, 2003] are relevant only to the later stages of a full precursory sequence and do not account for the initial evolution of crustal fracturing before bulk failure. Hence, an outstanding goal to understand the approach to bulk failure is to quantify relations between empirical exponential trends, such as equation (2), and the physical conditions of deformation.

2.2. Loading Conditions and Time-Dependent Behavior

[11] By focusing on creep deformation, studies of prefailure accelerations have removed applied stress as a time-related parameter. Time-dependent behavior has thus been attributed to a continued decrease in rock resistance under a constant load, caused by processes such as chemical corrosion by fluids [*Anderson and Grew*, 1977; *Atkinson*, 1984; *Lockner*, 1993; *Main and Meredith*, 1991], or increases in pore pressure. However, accelerating rates of rock fracturing also occur under different loading conditions. For example, when heterogeneous and crystalline crustal rocks (Table 1) are deformed under an increasing load at a constant strain rate, AEs frequently occur sporadically or maintain an approximately constant rate until reaching a threshold strain, which typically is about 50% of the strain at bulk failure [*Mogi*, 1962, 2007; *Scholz*, 1968; *Meredith et al.*, 1990], although values of 15%–75% have been observed [*Meredith et al.*, 1990]. At strains above the threshold, the AEs tend to accelerate exponentially with time (Figure 1) until the strain has reached ~90%–95% of the value at bulk failure, after which the acceleration becomes nonexponential and may instead follow a power law function [*Mogi*, 1962, 2007; *Scholz*, 1968; *Ohnaka and Mogi*, 1982; *Meredith et al.*, 1990; *Ojala et al.*, 2003]. The broad pattern therefore

Table 1. Physical Properties of Rocks for Interpreting AE Trends[a]

Rock	Reference	P_c (MPa)	$d\varepsilon/dt$ (10^{-5} s^{-1})	σ_{st} (MPa)	S^*_{AE} (MPa)	S^*_{calc} MJ m^{-3} (MPa)	ρ_b (kg m^{-3})	φ (%)	Modal Composition (vol %)									Average mole. wt (kg $mole^{-1}$)
									Qz	Mc	Or	PF	Px	Amph	Mica	Mt	Ch	
Pottsville Sandstone	*Scholz* [1968]	0	1	230	25	24	2541	3.0	46.4		41.0				10.9			0.27
Darley Dale Sandstone	*Meredith et al.* [1990], *Ismail and Murrell* [1976]	50	1	175	38	42	2357[b]	11.4	75.0			15.0[c]			10.0[d]			0.22
Darley Dale Sandstone	*Meredith et al.* [1990], *Ismail and Murrell* [1976]	200	1	480[e]	92	100	2357[b]	11.4	75.0			15.0[c]			10.0			0.22
San Marcos Gabbro	*Scholz* [1968]	0	1	215	19	19	2813	0.2				69.7	8.2	7.4	11.7			0.37
Shinkomatsu Andesite	*Ohnaka and Mogi* [1982]	0	0.1	82	13	19	2470	5.3				73.8	21.7			4.1		0.33
Mt. Shasta Andesite[f]	*Smith et al.* [2009]	10	1	105	29	38	2500[b]	7.0				85.0	3.0	12.0				0.34[g]
Westerly Granite	*Scholz* [1968]	0	1	282	27	25	2646	0.9	27.5	35.4		31.4			4.9			0.26
Westerly Granite	*Meredith et al.* [1990], *Meredith and Atkinson* [1985]	100	1	780	53	58	2646	1.0	27.0	36.0		30.0			7.0[h]			0.27
Red Aue Granite	*Zang et al.* [1998]	0	1	120	20	22	2620	1.3	30.0		20.0	40.0			10.0			0.29
Mannari Granite	*Ohnaka and Mogi* [1982]	0	0.01	150	24	23	2620	0.7	31.1		38.5	23.9		0.3	4.3	0.3	1.6	0.28
Rutland Quartzite	*Scholz* [1968]	0	1	505	56	51	2643	0.5	91.0	2.0	7.0							0.13

[a] P_c, confining pressure; $d\varepsilon/dt$, nominal bulk strain rate; σ_{st}, fracture stress in compression; S^*_{AE}, characteristic stress from AE data; S^*_{calc}, calculated reference energy per unit volume, $(3kT\phi + P_c)/3$; ρ_b, bulk density; φ, porosity; Qz, quartz; Mc, microcline (alkali feldspar); Or, orthoclase (alkali feldspar); PF, plagioclase feldspar (anorthite-albite); Px, pyroxene (augite-hypersthene); Amph, amphibole (hornblende); Mica, biotite-muscovite; Mt, magnetite; Ch, chlorite. See Table 2 for molecular weights of minerals. All samples were water-unsaturated except for Darley Dale sandstone, which was water-saturated.

[b] Bulk density calculated from composition and porosity.

[c] Combined value for PF and Mc.

[d] Mica used for unspecified "other" component.

[e] Stress at yielding to catasclastic flow, not brittle fracture.

[f] Temperature 300°C for Mt. Shasta Andesite, ambient value for all other experiments.

[g] Estimated from phenocryst percentages.

[h] Value includes 1% of unspecified "other" components.

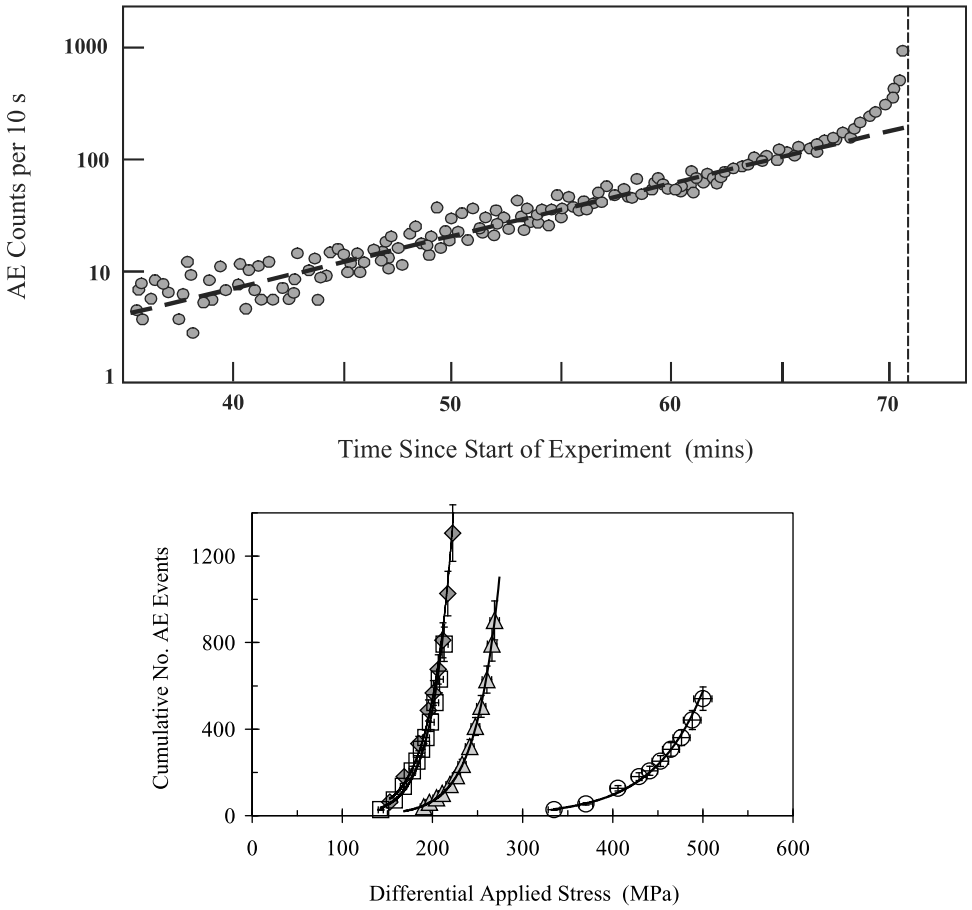

Figure 1. (top) Exponential increase in AE event rate with time (note the logarithmic scale for AE count rate). Data are for Shinkomatsu andesite at room temperature and pressure, loaded in compression at a nominal rate of 0.023 MPa s^{-1}. About 35 min after the start of the experiment, the AE rate converges on an exponential trend (gray dashed line), but follows a faster-than-exponential trend after about 67 min until bulk failure (vertical dashed line). Data from *Ohnaka and Mogi* [1982], see also Table 1. (bottom) Exponential increase in cumulative number of AE events with differential applied stress. The best fit trends have the form $\Sigma\nu = a \exp(bS)$. Respective values for a and b are 0.157 and 0.041 for Pottsville sandstone (diamonds), 0.014 and 0.054 for San Marcos gabbro (squares), 0.037 and 0.037 for Westerly granite (triangles), and 0.075 and 0.018 for Rutland quartzite. S in MPa. Data from *Scholz* [1968], see Table 1 for experimental conditions.

resembles that observed during accelerating creep (e.g., with α in equation (1) increasing from 1 to 2 as fracturing proceeds). However, unlike creep models, the strain and amount of fracturing cannot be assumed to change in proportion to each other. Analogous differences between changes in strain and recorded fracturing have also been observed before volcanic eruptions [*Bell and Kilburn,* 2011] (Figure 2). Thus, even if the Voight relation (equation (1)) may apply when setting Ω as the number of AEs, it does not apply if Ω is equated with strain (because the loading conditions impose a constant strain rate, so that the acceleration is zero and does not follow the relation in equation (1)).

[12] For noncreep loading, time-dependent fracturing and deformation have been introduced by changing the applied stress and so there is no immediate need to invoke mechanisms for reducing a rock's resistance. The increasing-load data thus provide an opportunity to investigate how brittle deformation is influenced by the intrinsic properties of rock, before including the effects of additional factors, such as the action of fluids. They will also provide insights into how physical conditions lead to the empirical descriptions of the approach to bulk failure.

3. Deformation Under Increasing Load

3.1. Variation of AEs With Stress and Strain

[13] It is not obvious that AE rates should show any preferred variation with time. For deformation under increasing load, this behavior is favored by the experimental constraint of a constant strain rate. Under simulated conditions for subvolcanic bedrock, sandstones and crystalline igneous rocks with vesicularities of a few vol % or less show quasi-elastic behavior (inelastic strain $\leq$ 5% of total strain) until the increase in AE rate becomes faster than exponential [*Meredith et al.*, 1990; *Lockner*, 1998; *Rocchi et al.*, 2004; *Smith et al.*, 2009]. Within experimental precision, therefore, the exponential increases in AE rate with time can be viewed as a response to either a constant strain rate or constant load rate, that is, time

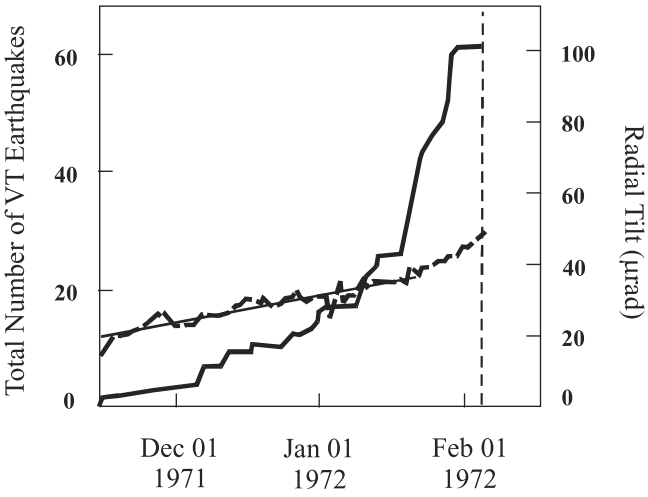

Figure 2. Contemporaneous changes with time in recorded numbers of volcanotectonic (VT) events (solid curve) and radial tilt (broken curve) before the 4 February 1972 eruption (vertical dashed line) of Mauna Ulu on Kilauea, Hawaii. The signals are field-scale proxies for AE and strain. The tilt rate remains approximately constant (continuous line) until the second half of January 1971, when it increases to a higher rate, which is also approximately constant. In contrast, the VT event rate accelerates throughout the precursory interval and is well described by a daily rate that increases in proportion to $e^{t/20}$, where t is time in days since the start of the precursory sequence (the fitting of trends is discussed in detail by *Bell and Kilburn* [2011]). Figure modified from *Bell and Kilburn* [2011]. Field data from *Klein* [1984], *Tilling et al.* [1987], and *Lengliné et al.* [2008].

is a proxy measure for bulk deformation or applied differential stress. Hence, assuming that the total number of fracturing events is proportional to the total number, $\Sigma\nu$, of AE [*Scholz*, 1968], then dimensional reasoning indicates that an exponential dependence of $\Sigma\nu$ on bulk strain or stress must take the general form:

$$\Sigma\nu/(\Sigma\nu)_m = \exp[(\varepsilon - \varepsilon_m)/\varepsilon^*] = \exp[(S_d - S_{dm})/S^*] \quad (4)$$

where S_d is bulk differential stress, which takes a value of S_{dm} when $\Sigma\nu = (\Sigma\nu)_m$, S^* is a characteristic stress, which will be identified below (Figure 3), the bulk strain $\varepsilon \approx S_d/Y$, $\varepsilon^* \approx S^*/Y$; Y is Young's modulus for elastic deformation, and the subscript m defines maximum values at the end of the exponential sequence.

[14] For equation (4) to be physically meaningful, the reference terms S_{dm}, S^*, ε_{dm}, and ε^* must be material properties that can be determined independently. The cumulative number of events achieves its maximum value when $S_d = S_{dm}$ and $\varepsilon = \varepsilon_m$. Given that the maximum number of AEs are obtained shortly before bulk fracture, it follows that the strength σ_{st} and strain at bulk failure ε_{st} are representative scales for S_{dm} and ε_m.

[15] The initial cumulative number of detected AEs is at least 10^{-2} of its maximum value [*Scholz*, 1968; *Ohnaka and Mogi*, 1982; *Meredith et al.*, 1990], for which the exponents in equation (4) become approximately $-\varepsilon_m/\varepsilon^*$ and $-S_m/S^*$ and take values of -5 or less ($e^{-5} \approx 10^{-2}$); S^* and ε^* must therefore be much less than S_{dm} and ε_m and so reflect a condition that is established before bulk failure. Noting that stress has units of energy per deformation per volume, an immediate possibility is that S^* is a measure of the reference amount of deformation that exists among atoms before a differential stress is applied.

[16] The ideal spacing between atoms is defined at absolute zero temperature and zero confining pressure [*Azároff*,

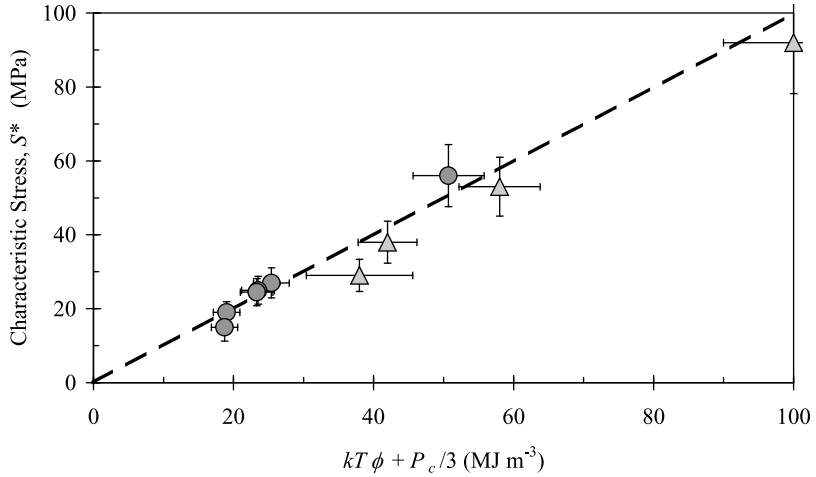

Figure 3. The characteristic stress, $S^* \approx (3kT\phi + P_C)/3$, which reduces to $S^* \approx kT\phi$ at atmospheric pressure (circles). Equality is shown by the broken line. Triangles show experiments at confining pressures between 10 and 200 MPa (Table 1). The data at high P_C suggest that the observed S^* may be about 10% less than calculated values, but additional measurements are required to confirm this relation. Rock properties and experimental conditions are given in Table 1 and, for experiments under ambient conditions, the temperature was set at 293 K (20°C). Where error bars are not visible, the symbol is larger than the error.

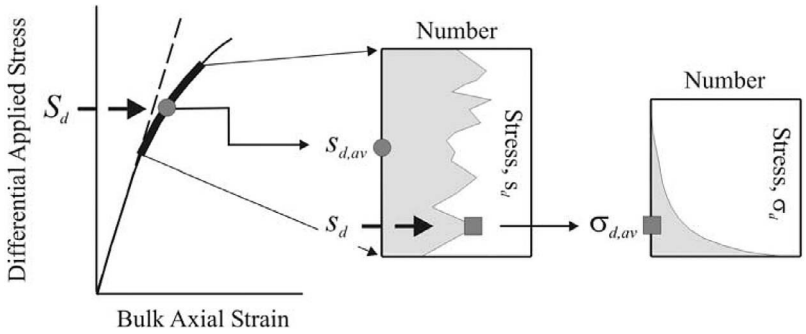

Figure 4. (left) Relations between applied stress and resulting strain for rock (continuous curve) and for ideal elastic behavior (broken line). The difference between them, which is produced by movements along discontinuities, has been exaggerated for clarity. In response to loading conditions and rock heterogeneity, external stresses are distributed unevenly throughout a sample and cover a range of values (thick section of curve) about the mean S_d, which corresponds to the value of the bulk applied differential stress. When S_d exceeds a threshold value, some of the higher stresses about the mean will be metastable at values greater than the fracture stress (right end of curve). Bulk failure occurs when S_d equals the fracture stress. See also Figure 5. (middle) The frequency distribution of macroscopic point stresses s_d is assumed to remain constant during episodes of exponential AE increase. The distribution is schematic for illustration. (right) Each macroscopic point contains a large population of atoms, among which the energy ($e_j = \sigma_j/\phi$) added by an external stress is distributed according to the Boltzmann distribution (see also Figure 5).

1960]. The spacing changes at temperatures and confining pressures above zero and represents a deformation with respect to ideal conditions. The additional effect on atomic spacing due to a differential stress also depends on the departure from the ideal spacing before the stress is applied. Therefore, it is anticipated that the relative deformation due to applying a differential stress can be measured in terms of the quantity (Energy supplied per volume per deformation because of an applied differential stress)/(Energy stored per volume because of a temperature and pressure above zero).

[17] Previous experimental studies have noted a temperature dependence on the amount of AEs or inelastic strain produced by a particular applied stress [*Lockner*, 1998; *Ojala et al.*, 2003]. The temperature dependence of S^* will thus be considered first. The additional influence of confining pressure will be addressed in section 3.3.

[18] At temperatures above absolute zero, atoms absorb thermal energy (E_{th}, which is also described as internal energy) and among solids, this energy allows atoms to adjust the distance from their neighbors and also to vibrate about their mean positions [*Azároff*, 1960]. For temperatures typical within Earth's crust (from surface to magmatic values), the internal energy per unit volume $E_{th}/V = 3kT\phi$ (J molecule^{-1}) [*Young*, 1992], where k is the Boltzmann constant (1.381×10^{-23} J molecule^{-1} K^{-1}), T is absolute temperature, and ϕ is the number of molecules per unit volume (molecules m^{-3}); ϕ is given by $\rho N_A/W_m$, where ρ and W_m are the rock's mean density and molar mass (kg mole^{-1}), and N_A is Avogadro's number (6.022×10^{23} molecules mole^{-1}). E_{th}/V excludes the energy from any significant confining pressure. Therefore, as a first test, Figure 3 shows the variation of S^* with E_{th}/V for the experiments run at atmospheric pressure and temperature (see also Table 1 for experimental conditions). The data yield $S^* \approx E_{th}/3V = kT\phi$ and confirm that S^* describes a physical rock property and is not an empirical constant; the corresponding quantity for ε^* is $kT\phi/Y$.

3.2. Atomic and Macroscopic Controls on Brittle Deformation

[19] Substituting the representative scales for S_{dm} and S^*, equation (4) becomes

$$\Sigma\nu/(\Sigma\nu)_m = \exp[(S_d - \sigma_{st})/kT\phi] \quad (5)$$

The term $S_d/kT\phi$ indicates that fracturing depends on how the supplied energy is accommodated at macroscopic and atomic scales (through S_d and $kT\phi$, respectively). Macroscopically, the applied stress is distributed unevenly within a sample as a result of the geometry of loading and of heterogeneities in the rock, such as cracks and crystals with different mechanical properties [*Scholz*, 1968]. Elasticity theory treats material as a continuum and determines the local values and orientations of differential stress s_d, which are considered to operate at points throughout the sample [*Jaeger*, 1969]. The values of s_d lie along the rock's macroscopic stress–strain curve about a mean value of S_d (Figure 4).

[20] Each macroscopic point describes an elementary volume V_e, which, although it is much smaller than the volume of rock being deformed, nevertheless, consists of a large number of atoms. For example, common crustal rock contains $\sim 6 \times 10^{27}$ atoms m^{-3} (determined from ϕ and the data in Table 1), so that even at length scales of $\sim$10 nm, V_e will contain $\sim 10^6$ atoms. The properties calculated for a macroscopic point thus describe the average behavior of a large number of atoms within that point. Hence, if σ_d denotes an effective differential stress acting across an atom, then the local differential stress s_d across V_e represents the average value of σ_d within that elementary volume.

[21] The values of s_d are imposed by macroscopic conditions, so that elementary volumes can be treated independently for determining the distribution of σ_d. When subjected to s_d, the atoms within an elementary volume can absorb a range of additional energy determined by quantum-mechanical

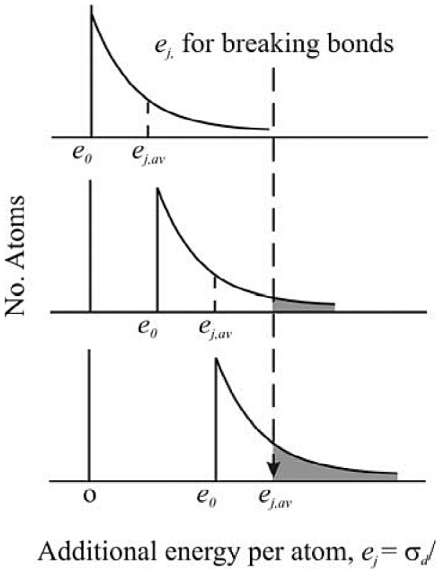

Figure 5. The Boltzmann distribution for the energy ($e_j = \sigma_j/\phi$) added by an external stress to atoms within a macroscopic point. (top to bottom) As the stress s_d increases, the distribution moves to larger values of e_j while retaining the same overall shape. Bonds with e_j larger than the breaking value are metastable and will eventually fail. The proportion of broken bonds is given by the ratio of the shaded area to the area of the whole distribution. Fracturing across a macroscopic point occurs when $e_{j,av}$ ($= \sigma_{j,av}/\phi = s_d/\phi$) reaches the breaking value. Compare with Figure 4.

constraints [*Azároff*, 1960; *Reif*, 1985; *Young*, 1992]. Assuming that each value in the range is equally likely to be selected (a fundamental postulate of statistical physics) [*Reif*, 1985], a large number of possible combinations exist in which the additional energy can be distributed. However, because an elementary volume is also constrained to accommodate a fixed amount of total additional energy from s_d (conservation of energy) among a fixed number of atoms (conservation of mass), it emerges that the number of atoms n_j with an additional energy e_j (associated with σ_d and defined below) is expected to be given by

$$n_j = n_0 \exp\left[-\left(e_j - e_0\right)/kT\right] \tag{6}$$

where n_0 is the number of atoms that acquire the minimum additional energy e_0.

[22] Equation (6) is an example of the classical Boltzmann distribution of molecular energy that underpins statistical physics [*Boltzmann*, 1872] and, as a result, it is also referred to as the canonical distribution [e.g., *Reif*, 1985, chap. 6 and 7; *Ruhla*, 1992, chap. 5; *Guénault*, 1995, chap. 2]. The distribution connects the macroscopic properties of materials to the statistical averages of a range of energy states at the atomic level. The particular energy states involved depend on the macroscopic properties being described, but well-known expressions based on the Boltzmann distribution include formulae for calculating gas pressure [*Ruhla*, 1992], specific heat of solids [*Einstein*, 1907], viscosity of liquids [*Glasstone et al.*, 1941], rates of chemical reactions [*Glasstone et al.*, 1941; *Frank-Kamenetski* , 1969], and the onset of thermal explosions in liquids and solids [*Bowden and Yoffe*, 1952].

[23] Equation (6) contains no upper limit on the value of e_j. The ideal distribution thus includes atoms that can acquire additional energies greater than the value e_{st} associated with the breaking strength of a bond (Figure 5). Such bonds are metastable and are expected to fail. Hence, for a given value of e_j, the number of atoms n_b with a broken bond is given by integrating equation (6) for $e_j \geq e_{st}$ to yield

$$n_b = n_0\, kT \exp[-(e_{st} - e_0)/kT] \tag{7}$$

The energy consumed in breaking bonds decreases the local stress acting over an elementary volume. The local stress-drop is recovered when the stress imposed on the whole rock remains unchanged or increases. Each elementary volume reestablishes a Boltzmann distribution of additional energy among its atoms, so that further bonds can break where the energy acquired exceeds e_{st}. Hence, bonds continue to be broken until the externally imposed stress is reduced.

[24] The exponential terms in equations (5)–(7) are connected by relations between σ_d, s_d, and S_d. At the atomic scale, the energy $e_{\Delta r}$ required to change the spacing between atoms in a particular direction by an amount Δr is given by $\pi r_0^2(\sigma_i/2)\Delta r_i$, which is the product of the mean additional force ($\pi r_0^2(\sigma_i/2)$) and change in equilibrium spacing (Δr_i), r_0 is the equilibrium spacing between atoms at temperature T before application of an external stress (when $S_d = 0$), and the subscript i denotes the direction of the force. The effective differential stress, σ_d, is the difference between the highest and lowest principal stresses, $\sigma_1 - \sigma_3$. Numerically, it is given by $\sigma_1 - \sigma_3 = 8/3[(e_{\Delta r_1}/\varepsilon_{\Delta r_1}) - (e_{\Delta r_3}/\varepsilon_{\Delta r3})](3/4\pi r_0^3)$, which highlights that σ_d is proportional to the difference in energy per unit strain ($\varepsilon_{\Delta r_i} = \Delta r_i/r_0$) per unit volume ($4\pi r_0^3/3$) supplied along the directions of greatest and least principal stresses; in terms of difference in energy supplied per unit strain per atom, it can be expressed alternatively as σ_d/ϕ, which, with dimensions of energy per atom, is identified with e_j in equation (6).

[25] After manipulation and integration between $n_j = 0$ and n_0, equation (6) yields $e_{j,av} = kT + e_0$. Given that kT is constant for a particular episode of deformation, the term for minimum additional energy e_0 is seen to increase with $e_{j,av}$, which is equivalent to the point stress s_d. Substituting for e_0 in equation (7) then leads to $n_b = n_0$ [exp (−1)] kT exp $[-(\sigma_{st} - s_d)/kT\phi]$, which shows that the number of atoms with broken bonds in an elementary volume increases exponentially with s_d. Hence, in a sample that consists of a collection of elementary volumes, each with the same number of atoms, n_e, the total number of atoms with broken bonds, N_b, becomes $N_b = n_0$ [exp (−1)] kT [exp $-(\sigma_{st}/kT)\phi$] $\Sigma_{\text{all } sd}$ [exp $(s_d/kT\phi)$]. Introducing α as the difference between an individual point stress and the mean value S_d for the whole sample (Figure 4), then $s_d = S_d + \alpha$ and the summation of exp $(s_d/kT\phi)$ can be rewritten as [exp $(S_d/kT\phi)$] $\Sigma_{\text{all } \alpha}$ exp $(\alpha/kT\phi)$. Assuming that the distribution of s_d about the mean remains the same during deformation, then the distribution of α must also remain the same, so that $\Sigma_{\text{all } \alpha}$ exp $(\alpha/kT\phi)$ is a constant, K, for any given sample. Hence, substituting for s_d yields

$$n_b = K\, n_0[\exp(-1)]kT[\exp(S_d - \sigma_{st})/kT\phi] \tag{8}$$

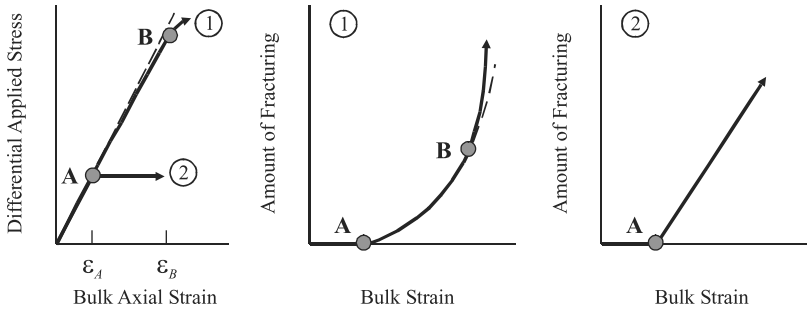

Figure 6. (left) Idealized stress–strain relations (solid curves) for compression under an increasing stress (curve 1) and a constant stress after a strain ε_A has been exceeded (curve 2). Curve 1 deviates from the elastic trend (dashed line) by only a small amount until it is strained beyond position B; curve 2 deviates significantly when it is strained beyond position A. The amount of deviation is proportional to the total amount of fracturing. (middle) Under increasing stress, curve 1 shows elastic deformation without fracturing at strains less than the value at A, after which the amount of fracturing increases exponentially with strain and, beyond point B, at a rate that is faster than exponential (the dashed curve shows the extrapolation of the exponential trend). (right) For creep, curve 2 shows elastic deformation without fracturing at strains less than the value at A, after which the amount of fracturing increases in proportion with strain (which increases under a constant load). Points A and B show corresponding locations between the stress–strain and rate diagrams.

For a total number N_{Tot} of atoms in a sample, the ratio N_b/N_{Tot} describes the expected proportion of broken bonds. As N_b/N_{Tot} is proportional to exp $[(S_d - \sigma_{st})/kT\phi]$ (because N_{Tot} is constant), it follows that the exponential term describes the probability of bond failure and that $(\sigma_{st} - S_d)/\phi$ behaves as the mean activation energy per atom required for breaking bonds.

[26] Bulk failure occurs when $S_d = \sigma_{st}$, so that equation (8) can be simplified to $N_b/N_{bm} = \exp[(S_d - \sigma_{st})/kT\phi]$, where N_{bm} is the maximum value of N_b. Assuming that the total number of detected AEs is proportional to the number of atoms with broken bonds, then $N_b/N_{bm} = \Sigma\nu/(\Sigma\nu)_m$ and replacing $kT\phi$ with S^*, equation (8) leads to

$$\Sigma\nu/(\Sigma\nu)_m = \exp[(S_d - \sigma_{st})/S^*] = \exp[(\varepsilon - \varepsilon_{st})/\varepsilon^*] \quad (9)$$

which are identical to the relations inferred from observation (equation (4)) and confirm that the evolution of brittle deformation is determined by the distribution of strain energy at the atomic scale, through S^* and ε^*, as well as macroscopically through S_d and ε. Thus, elasticity theory describes the distribution of stresses and strains among macroscopic points and so identifies zones of stress concentration where local fracturing is expected (such as at crack tips). At the same time, the quantum behavior of atoms describes the distribution of additional energy within a macroscopic point and determines the probability that fracturing will occur at that point.

3.3. The Influence of Confining Pressure

[27] The ideal spacing between atoms is defined at zero confining pressure, P_C, as well as at absolute zero. Before a differential stress is applied, therefore, the reference energy per unit volume that describes the deviation from ideal conditions is given by $(E/V) + P_C$, so that a more complete expression for S^* is $(3kT\phi + P_C)/3$. At atmospheric pressure, $P_C/3$ can be neglected (<0.0025 $kT\phi$), for which $S^* \approx kT\phi$, as before. The full expression for S^* is consistent with additional experimental data for sandstone and igneous rocks under confining pressures of as much as 200 MPa (Figure 3, Table 1). Equations (4) and (9) are thus expected to apply down to depths of at least 8 km (P_C = 200 MPa).

4. Connecting Physical and Empirical Models

[28] Changes in the number or fracturing events with time can be obtained from equation (9) by explicitly incorporating the time dependence of applied stress. Thus, for a stress that increases linearly with time, $S_D = S_{init} + K_S t$ where S_{init} is the differential stress at the start of observation and K_S is the constant stress rate. Differentiating equation (9) with respect to time yields $d\Sigma\nu/dt = (\Sigma\nu)_m (K_S/S^*) \exp[(K_S t - \sigma_{st})/S^*]$ and $d^2\Sigma\nu/dt^2 = (\Sigma\nu)_m (K_S/S^*)^2 \exp[(K_S t - \sigma_{st})/S^*]$, so that

$$d^2\Sigma\nu/dt^2 = (K_S/S^*)d\Sigma\nu/dt \quad (10)$$

Equation (10) has the form of the Voight relation (equation (1)) for exponential trends (α = 1); indeed, the two become the same if Ω is equated with $\Sigma\nu$ and A with K_S/S^*, which indicates that A depends on the composition of the rock, the temperature, and confining pressure at which it is deformed (all contributing to S^*), and on the rate of increase in applied stress (K_S).

[29] However, it is not evident that the equations should be equivalent, because they were determined for different sets of loading conditions. The simplest interpretation is that the Voight relation for accelerating creep can be applied to a wider range of loading conditions than originally proposed. If so, it follows that equation (10) and, hence, equation (9) may also be applicable to a broader range of loading conditions. For example, if rock resistance during creep is assumed to decrease linearly with time, such that the effective strength σ_{st} changes from its initial value $\sigma_{st,init}$ as $\sigma_{st} = \sigma_{st,init} - K_w t$ (where K_w is the constant rate of weakening), then equation (9) becomes $\Sigma\nu/(\Sigma\nu)_m = \exp\{[S_d - (\sigma_{st,init} - K_w t)]/S^*\} = \exp[(S_d - \sigma_{st,init} +$

Table 2. Representative Molecular Weights for Selected Minerals

Mineral	Composition[a]	Number of Framework O Atoms per Molecule, Excluding OH	Mole Weight (kg mole^{-1})
Quartz	SiO_2	4	0.12
Alkali feldspar (orthoclase and microcline)	K Al Si_3 O_8	8	0.28
Plagioclase feldspar (anorthite to albite)	Ca Al_2 Si_2 O_8 − Na Al Si_3 O_8	8	0.27 ± 0.01
Pyroxene (augite and hypersthene)	Mg_2 (Si $Al)_2$ O_6 − Fe_2 (Si $Al)_2$ O_6	6	0.23 ± 0.03
Amphibole (hornblende)	Ca_2 $(MgFe)_5$ Al_2 Si_6 O_{22} $(OH)_2$ − Ca_2 $(MgFe)_3$ Al_4 Si_6 O_{22} $(OH)_2$	22	0.83 ± 0.08
Mica (biotite-muscovite)	K_2 (Mg Fe $Al)_6$ Si_8 O_{20} $(OH)_4$ − K_2 Al_4 Si_8 O_{20} $(OH)_4$	20	0.9 ± 0.1
Magnetite	Fe^{2+} Fe_2^{3+} O_4	32	1.85
Chlorite	$(Mg, Al, Fe)_{12}$ $(Si, Al)_8$ O_{20} $(OH)_{16}$	20	1.3 ± 0.2

[a]Mineral Formulae From *Deer et al.* [1966].

$K_w t)/S^*$]. Hence, differentiating with respect to time as for equation (10) leads to

$$d^2\Sigma\nu/dt^2 = (K_w/S^*)d\Sigma\nu/dt \quad (11)$$

which is identical to the Voight relation for creep with $\alpha = 1$, $\Omega \equiv \Sigma\nu$, and $A \equiv K_w/S^*$. In this case, therefore, A depends on the rate of rock weakening and on rock composition, temperature, and confining pressure.

[30] Equation (9) thus naturally yields exponential rates of rock fracturing with time before bulk failure in compression for at least two simple loading conditions: a load increasing at a constant rate of stress or strain and a constant load with a constant rate of rock weakening. The two loading conditions, however, are associated with different time-dependent changes in the accompanying rates of deformation. For accelerating creep, fracturing and deformation are expected to change in proportion to each other [*Voight*, 1988], whereas fracturing rate increases exponentially with time when the rate of deformation is held constant. The differences in behavior can be explained by noting that the total strain ε is the sum of elastic ε_{el} and inelastic ε_{in} components and assuming that ε_{in} is proportional to the total amount of fracturing ($\varepsilon_{in} = B\Sigma\nu$, where B is a constant). Hence, $\varepsilon = \varepsilon_{el} + B\Sigma\nu$ and so deformation rate $d\varepsilon/dt$ becomes

$$d\varepsilon/dt = d\varepsilon_{el}/dt + Bd\Sigma\nu/dt \quad (12)$$

For the experiments under increasing load, inelastic deformation is much smaller than the elastic component for strains less than about 90% of the strain at bulk failure (section 3; Figure 6). The strain rate is then well approximated by $d\varepsilon_{el}/dt$, which by definition is proportional to dS_d/dt and so is constrained to be constant by experimental conditions. In contrast, deformation during creep is controlled by the inelastic component (Figure 6), so that the strain rate is well approximated by $Bd\Sigma\nu/dt$ (= $d\varepsilon_{in}/dt$), yielding the expected proportionality between rates of strain and fracturing.

5. Discussion

5.1. The Locations of Activated Cracks in Laboratory Samples

[31] At atmospheric pressure, the parameters S^* and ε^* that characterize the exponential trends in equations (4) and (9) are proportional to a rock's internal energy and have been determined from the composition of a whole sample, rather than that of a particular mineral. Internal energy is inversely proportional to molecular weight. The average molecular weights lie between 0.27 and 0.37 kg mole^{-1} for the rock samples (Table 1) and between 0.12 and 0.90 kg mole^{-1} for individual mineral phases (Table 2). The observation that average internal energy is a representative quantity thus suggests either that (1) the activation of discontinuities occurs preferentially in minerals with molecular weights also in the range 0.27–0.37 kg mole^{-1}, which broadly corresponds with the feldspars that are a major component of the studied rocks (Table 2), or (2) discontinuities are located throughout a sample independent of local composition and so the mean internal energy of the adjacent rock reflects the average value for the whole sample.

5.2. Application of Model to Damage Mechanics

[32] Equation (9) relates the number of cracking events to the bulk applied stress and bulk strain. An alternative description for relating cracking to bulk parameters utilizes the so-called damage parameter D, which describes the differences between observed and ideal elastic conditions through changes in the effective modulus of elasticity of cracked rock. Thus, if Y is the Young's modulus of uncracked rock, then the effective modulus Y' for cracked rock is given by $Y(1 - D)$ [*Turcotte et al.*, 2003; *Lemaitre and Desmorat*, 2005]. Thus, the bulk strain $\varepsilon = S_D/Y'$ and elastic strain $\varepsilon_{el} = S_D/Y$. Hence, because inelastic strain (ε_{in}) is the difference between the bulk and elastic strains, it follows that $\varepsilon_{in} = S_D/Y' - S_D/Y = D\varepsilon$, from which $D = \varepsilon_{in}/\varepsilon$. Hence, for inelastic strain proportional to the total number of fracture events, equation (9) yields $D \propto (1/\varepsilon) \exp[(S_d - \sigma_{st})/S^*] \propto (1/\varepsilon) \exp[(\varepsilon - \varepsilon_{st})/\varepsilon^*]$ and, for the special condition of deformation under constant rates of strain (K_ε), $D \propto (1/K_\varepsilon t) \exp(K_\varepsilon t/S^*)$.

5.3. Application of Model to Different Scales and Stress Fields

[33] Internal energy and confining pressure do not depend on the scale of observation and so their appearance as controlling parameters suggests that the laboratory relations can be extended to larger length scales, provided that the model's assumptions about macroscopic behavior also remain valid. Application of the model must therefore satisfy the explicit assumptions that (1) discontinuities and mechanical heterogeneities in rock occupy volumes much smaller than the amount of rock being deformed, (2) the distribution of macroscopic stresses about the mean remains the same during deformation, and (3) the total amount of fracturing is proportional to the total number of detected fracturing events.

[34] The first assumption is the most likely to be compromised and will fail when continuous, mechanically distinct zones occupy a significant fraction of the total volume. This may occur, for example, among samples that contain inclusions of specific minerals or, at the field scale, when the deforming crust contains significant zones that have been selectively altered, such as by thermal processes or reactions with circulating fluids in volcanic districts. They will also occur when the volume contains one or more throughgoing discontinuities before deformation begins. In all such cases, the overall variation of fracturing with stress or deformation may deviate from the expected exponential trend. The deviations, however, may appear as local anomalies within the volume being deformed, in which case it may be possible to remove them by using appropriate spatial-filtering techniques.

[35] Application of the exponential model must further satisfy the constraint that cracking is controlled by changes imposed on a rock and not by any self-feeding interactions among cracks. This constraint is implicit when attributing time-dependent behavior only to rates of change in applied stress or in effective rock weakening because it neglects the potential for fracturing itself to promote further fracturing without any change in imposed conditions. This potential is controlled by the accumulation of strain energy stored in rock surrounding a crack tip [*Griffith*, 1921]. As a crack grows under a constant or increasing applied stress, the strain energy stored ahead of its tip becomes larger. Eventually, the crack reaches a critical length, above which the amount of stored energy is large enough to promote further growth. At this stage, the crack can continue to grow unhindered, provided the applied stress does not decrease or the crack tip does not encounter an obstacle produced by mechanical heterogeneity. It is thus expected that, as cracks grow, the conditions for self-accelerating crack growth will be met before bulk failure.

[36] Indeed, the onset of self-accelerating cracking has been associated with two features that emerge shortly before bulk failure: (1) the appearance of faster-than-exponential increases in rates of fracturing [*Kilburn*, 2003] and (2) a change from distributed cracking throughout a sample to the localization of cracking within a small volume in which the eventual plane of failure develops as a sample fails [*Hallbauer et al.*, 1973; *Lockner et al.*, 1991]. A progression from exponential to faster-than-exponential trends suggests that the second trend has the potential of being described by an extension of the present analysis. This could possibly be accommodated quantitatively by applying mean-field theory to express the average additional energy available locally for crack growth [*Main*, 1991; *Kilburn*, 2003] and to incorporate the new term as an effective increase in the mean deforming stress in equation (9). The effect of localization could also be accommodated by adjusting the distribution of macroscopic stresses about the mean, provided that the new distribution remains the same until bulk failure (so satisfying assumption (2)). Such an extension of the present analysis will be considered elsewhere.

5.4. Using Time Series to Identify Loading Conditions

[37] Although the AE trends have been tested against experimental data in compression, their derivation has not required the stresses to be compressive, and so the results are expected to be applicable to other stress regimes. Indeed, the potential validity of the model for extensional deformation is implied by studies that have used the Voight relation to describe the behavior of crust being stretched at volcanoes before eruptions [*Voight*, 1988; *De la Cruz-Reyna and Reyes-Davila*, 2001; *Kilburn*, 2003; *Smith et al.*, 2009; *Bell and Kilburn*, 2011].

[38] When applied stress or rock resistance vary linearly with time, equation (9) yields the rates of fracturing and strain observed during deformation under increasing load and during accelerating creep (section 4). Equation (9) may thus represent a parent relation from which time series for fracturing and strain can be forecast if the general time dependence of loading and weakening are known. For example, if $f(t_S)$ and $g(t_w)$ denote the variation of applied stress and rock weakening with time, equation (9) can be used to infer

$$\Sigma\nu/(\Sigma\nu)_m = \exp[(f(t_S) - f(t_w))/S^*] \quad (13)$$

In principle, equation (13) may describe complex changes in fracturing with time, according to the particular forms of $f(t_S)$ and $g(t_w)$. However, modeling by *Main* [2000] and experiments on sandstone by *Ojala et al.* [2003] have shown that combined failure by corrosion (controlling $g(t_w)$) under approximately constant loading rates (controlling $f(t_S)$) can also yield simple trends that, similar to Voight's model (equation 1), are consistent with either exponential or power function increases in the rate of cracking with time.

[39] Conversely, the combined behavior of fracturing and deformation with time has the potential for inferring the type of loading when the stress–strain conditions are not known beforehand. Thus, as illustrated in Figure 6, a similar type of time dependence for both fracturing and strain would be consistent with rock creep, whereas the combination of an exponential increase in the rate of fracturing and constant rate of strain would indicate deformation under an increasing stress.

[40] For example, *Bell and Kilburn* [2011] found that, of the 57 seismic precursory sequences recorded before eruptions and intrusions at Kilauea, Hawaii, between 1960 and 1983, almost one-third were characterized by exponential increases with time in the numbers of VT events (analogous to AE). A comparable data set has yet to be compiled of contemporaneous rates of deformation. However, suitable data were obtained for deformation during four of the exponential seismic increases and all indicated an approximately constant strain rate. Figure 2 shows a representative example from the eruption on 4 February 1972. Compared with Figure 6, the pairs of observed trends suggest that, in these particular cases, the precursory trends were controlled by an increase in applied stress, rather than by creep failure.

6. Conclusion

[41] At pressures and temperatures that occur in at least the upper 8 km of the crust, including volcanic environments, mechanically heterogeneous, crystalline rocks may deform and fracture at an accelerating rate as they approach bulk failure. For constant rates of compression, the amount of fracturing commonly increases exponentially with applied stress or total strain for strains between a few tens of percent and about 90% of the value at bulk failure. The exponential

behavior is controlled by quantum constraints in distributing energy among atoms (equations (6) and (7)) and appears macroscopically when the local stresses maintain a similar distribution about their mean value (equivalent to the applied differential stress; Figure 5). The term characterizing the exponential trend (denoted by S^* or ε^* in equation (9)) depends on rock composition, temperature, and confining pressure, whereas the rate of fracturing depends, in addition, on the time rate of change of applied stress or rock resistance (equations (10) and (11)).

[42] The exponential trend between fracturing and stress or strain appears to be robust, independent of silicate rock composition, confining pressure, water saturation, and strain rate. Hence, subject to the constraints identified in section 5.2 (notably that discontinuities are much smaller than the volume being deformed, are distributed randomly in all directions, and do not interact with each other), equation (9) is also expected to apply (1) to all length scales and so be relevant to field studies, as well as to laboratory conditions, and (2) to failure in stress fields other than compression. The model, however, has been tested here only with experimental data for compressional failure at constant load rate or strain rate (Table 1) and, by analogy with the Voight relation (equation (1)), also under a constant load. A preliminary application to seismic and deformation trends before eruptions and intrusions in Hawaii (compiled by *Bell and Kilburn* [2011]) suggests that exponential trends in the numbers of precursory VT events are consistent with deformation under an increasing stress, rather than by creep. Further verification is required from experiments on a wider range of rock composition and deformation histories, as well as on data obtained in the field. Once the limits of validity have been established, complementary expressions can be developed for quantifying relations between fracturing, stress, and strain under a broader range of conditions.

[43] **Acknowledgments.** Philip Meredith (UCL) provided thoughtful discussions and insights into rock deformation in the laboratory. Thanks are due also to Ian Main (Edinburgh) and an anonymous reviewer, whose comments improved the manuscript. The research was privately funded.

References

Anderson, O. L., and P. C. Grew (1977), Stress corrosion theory of crack propagation with applications to geophysics, *Rev. Geophys.*, *15*, 77–104, doi:10.1029/RG015i001p00077.

Atkinson, B. K. (1984), Subcritical crack growth in geological materials, *J. Geophys. Res.*, *89*, 4077–4114, doi:10.1029/JB089iB06p04077.

Azároff, L. V. (1960), *Introduction to Solids*, McGraw-Hill, New York.

Bell, A. F., and C. R. J. Kilburn (2011), Precursors to dyke-fed eruptions at basaltic volcanoes: Insights from patterns of volcano-tectonic seismicity at Kilauea volcano, Hawaii, *Bull. Volcanol.*, doi:10.1007/s00445-011-0519-3, in press.

Benson, P. M., B. D. Thompson, P. G. Meredith, S. Vinciguerra, and R. P. Young (2007), Imaging slow failure in triaxially deformed Etna basalt using 3D acoustic-emission location and X-ray computed tomography, *Geophys. Res. Lett.*, *34*, L03303, doi:10.1029/2006GL028721.

Boltzmann, L. (1872), Weitere Studien ueber das Waemegleichgewicht unter Gasmolekuelen, *Wien. Ber.*, *66*, 275–370.

Bowden, F. P., and A. D. Yoffe (1952), *The Initiation and Growth of Explosion in Liquids and Solids*, Cambridge Univ. Press, Cambridge, U. K.

Burlini, L., S. Vinciguerra, G. Di Toro, G. De Natale, P. Meredith, and J.-P. Burg (2007), Seismicity preceding volcanic eruptions: New experimental insights, *Geology*, *35*, 183–186, doi:10.1130/G23195A.1.

Charles, R. J., and W. B. Hillig (1962), The kinetics of glass failure by stress corrosion, paper presented at Symposium sur la resistance mechanique du verre et les moyens de l'ameliorer, Union Sci. Cont. du Verre, Charleroi, Belgium.

Cornelius, R. R., and P. A. Scott (1993), A materials failure relation of accelerating creep as empirical description of damage accumulation, *Rock Mech. Rock Eng.*, *26*, 233–252, doi:10.1007/BF01040117.

Deer, W. A., R. A. Howie, and J. Zussman (1966), *An Introduction to the Rock Forming Minerals*, Longman, London.

De la Cruz-Reyna, S., and G. A. Reyes-Davila (2001), A model to describe precursory material-failure phenomena: Applications to short-term forecasting at Colima volcano, Mexico, *Bull. Volcanol.*, *63*, 297–308, doi:10.1007/s004450100152.

Dzurisin, D. (2007), *Volcano Deformation*, Springer, Chichester, U. K.

Einstein, A. (1907), Die Planckschе Theorie der Strahlung ueber die Theorie des Spezifischen Warme, *Ann. Phys.*, *22*, 180–190.

Frank-Kamenetskii, D. A. (1969), *Diffusion and Heat Transfer in Chemical Kinetics*, Plenum, New York.

Fukuzono, T. (1985), A method to predict the time of slope failure caused by rainfall using the inverse number of velocity of surface displacement, *J. Jpn. Landslide Soc.*, *22*, 8–13(in Japanese with English abstract).

Glasstone, S., K. J. Laidler, and H. Eyring (1941), *Theory of Rate Processes*, McGraw-Hill, New York.

Griffith, A. A. (1921), The phenomenon of rupture and flow in solids, *Philos. Trans. R. Soc. London A*, *221*, 163–198, doi:10.1098/rsta.1921.0006.

Guénault, A. M. (1995), *Statistical Physics*, 2nd ed., Kluwer, Dordrecht, Netherlands, doi:10.1007/978-1-4020-5975-9.

Hallbauer, D. K., H. Wagner, and N. G. W. Cook (1973), Some observations concerning the microscopic and mechanical behaviour of quartzite specimens in stiff, triaxial compression tests, *Int. J. Rock Mech.*, *10*, 713–726, doi:10.1016/0148-9062(73)90015-6.

Ismail, I. A. H., and S. A. F. Murrell (1976), Dilatancy and the strength of rocks containing pore water under undrained conditions, *Geophys. J. Astron. Soc.*, *44*, 107–134.

Jaeger, J. C. (1969), *Elasticity, Fracture and Flow*, 3rd ed., Chapman and Hall, London.

Kilburn, C. R. J. (2003), Multiscale fracturing as a key to forecasting volcanic eruptions, *J. Volcanol. Geotherm. Res.*, *125*, 271–289, doi:10.1016/S0377-0273(03)00117-3.

Kilburn, C. R. J., and D. N. Petley (2003), Forecasting giant, catastrophic slope collapse: Lessons from Vajont, Northern Italy, *Geomorphology*, *54*, 21–32, doi:10.1016/S0169-555X(03)00052-7.

Kilburn, C. R. J., and B. Voight (1998), Slow rock fracture as eruption precursor at Soufriere Hills volcano, Montserrat, *Geophys. Res. Lett.*, *25*, 3665–3668, doi:10.1029/98GL01609.

Klein, F. W. (1984), Eruption forecasting at Kilauea volcano, Hawaii, *J. Geophys. Res.*, *89*, 3059–3073, doi:10.1029/JB089iB05p03059.

Lei, X., K. Masuda, O. Nishizawa, L. Jouniaux, L. Liu, W. Ma, T. Satoh, and K. Kusunose (2004), Detailed analysis of acoustic emission activity during catastrophic fracture of faults in rock, *J. Struct. Geol.*, *26*, 247–258, doi:10.1016/S0191-8141(03)00095-6.

Lemaitre, J., and R. Desmorat (2005), *Engineering Damage Mechanics*, Springer, Berlin.

Lengliné, O., D. Marsan, J. L. Got, V. Pinel, V. Ferrazzini, and P. G. Okubo (2008), Seismicity and deformation induced by magma accumulation at three basaltic volcanoes, *J. Geophys. Res.*, *113*, B12305, doi:10.1029/2008JB005937.

Lockner, D. A. (1993), Room temperature creep in saturated granite, *J. Geophys. Res.*, *98*, 475–487, doi:10.1029/92JB01828.

Lockner, D. A. (1995), Rock failure, in *Rock Physics and Phase Relations*, *AGU Ref. Shelf*, vol. 3, edited by T. J. Ahrens, pp. 127–147, AGU, Washington, D. C.

Lockner, D. A. (1998), A generalised law for brittle deformation of Westerly Granite, *J. Geophys. Res.*, *103*, 5107–5123, doi:10.1029/97JB03211.

Lockner, D. A., J. D. Byerlee, V. Kuksenko, A. Ponomarev, and A. Sidorin (1991), Quasi-static fault growth and shear fracture energy in granite, *Nature*, *350*, 39–42, doi:10.1038/350039a0.

Main, I. G. (1991), A modified Griffith criterion for the evolution of damage with a fractal distribution of crack lengths: Application to seismic event rates and *b*-values, *Geophys. J. Int.*, *107*, 363–372, doi:10.1111/j.1365-246X.1991.tb00831.x.

Main, I. G. (1999), Applicability of time-to-failure analysis to accelerated strain before earthquakes and volcanic eruptions, *Geophys. J. Int.*, *139*, F1–F6, doi:10.1046/j.1365-246x.1999.00004.x.

Main, I. G. (2000), A damage mechanics model for power-law creep and earthquake aftershock and foreshock sequences, *Geophys. J. Int.*, *142*, 151–161, doi:10.1046/j.1365-246x.2000.00136.x.

Main, I. G., and P. G. Meredith (1991), Stress corrosion constitutive laws as a possible mechanism for intermediate-term and short-term seismic quiescence, *Geophys. J. Int.*, *107*, 363–372, doi:10.1111/j.1365-246X.1991.tb00831.x.

McGuire, W. J., and C. R. J. Kilburn (1997), Forecasting volcanic events: Some contemporary issues, *Geol. Rundsch.*, *86*, 439–445, doi:10.1007/s005310050152.

McNutt, S. R. (1996), Seismic monitoring and eruption forecasting of volcanoes: A review of the state-of-the-art and case histories, in *Monitoring and Mitigation of Volcano Hazards*, edited by R. Scarpa and R. I. Tilling, pp. 99–146, Springer, Berlin.

Meredith, P. G., and B. K. Atkinson (1985), Fracture toughness and subcritical cracks growth during high-temperature tensile deformation of Westerly granite and Black gabbro, *Phys. Earth Planet. Inter.*, *39*, 33–51, doi:10.1016/0031-9201(85)90113-X.

Meredith, P. G., I. G. Main, and C. Jones (1990), Temporal variations in seismicity during quasi-static and dynamic rock failure, *Tectonophysics*, *175*, 249–268, doi:10.1016/0040-1951(90)90141-T.

Mogi, K. (1962), Study of elastic shocks caused by the fracture of heterogeneous materials and its relation to earthquake phenomena, *Bull. Earthquake Res. Inst.*, *40*, 125–173.

Mogi, K. (2007), *Experimental Rock Mechanics*, Taylor and Francis, London.

Ohnaka, M., and K. Mogi (1982), Frequency characteristics of acoustic emission in rocks under uniaxial compression and its relation to the fracturing process to failure, *J. Geophys. Res.*, *87*, 3873–3884, doi:10.1029/JB087iB05p03873.

Ojala, I. O., B. T. Ngwenya, I. G. Main, and S. C. Elphick (2003), Correlation of microseismic and chemical properties of brittle deformation in Locharbriggs sandstone, *J. Geophys. Res.*, *108*(B5), 2268, doi:10.1029/2002JB002277.

Reif, F. (1985), *Fundamentals of Statistical and Thermal Physics*, McGraw-Hill, Singapore.

Rocchi, V., P. Sammonds, and C. R. J. Kilburn (2004), Fracturing of Etnean and Vesuvian rocks at high temperatures and low pressures, *J. Volcanol. Geotherm. Res.*, *132*, 137–157, doi:10.1016/S0377-0273(03)00342-1.

Roman, D. C., and K. V. Cashman (2006), The origin of volcanotectonic earthquake swarms, *Geology*, *34*, 457–460, doi:10.1130/G22269.1.

Ruhla, C. (1992), *The Physics of Chance*, Oxford Univ. Press, Oxford.

Saito, M. (1968), Forecasting the time of occurrence of a slope failure by tertiary creep [in Japanese], *J. Jpn. Landslide Soc.*, *4*, 1–8.

Scandone, R., and L. Giacomelli (2008), Precursors of eruptions at Vesuvius (Italy), *J. Volcanol. Geotherm. Res.*, *171*, 191–200, doi:10.1016/j.jvolgeores.2007.11.018.

Scholz, C. H. (1968), Microfracturing and the inelastic deformation of a rock in compression, *J. Geophys. Res.*, *73*, 1417–1432, doi:10.1029/JB073i004p01417.

Scholz, C. H. (2002), *The Mechanics of Earthquakes and Faulting*, 2nd ed., Cambridge Univ. Press, Cambridge, U. K.

Smith, R., and C. R. J. Kilburn (2010), Forecasting eruptions after long repose intervals from accelerating rates of rock fracture: The June 1991 eruption of Mount Pinatubo, Philippines, *J. Volcanol. Geotherm. Res.*, *191*, 129–136, doi:10.1016/j.jvolgeores.2010.01.006.

Smith, R., P. R. Sammonds, and C. R. J. Kilburn (2009), Fracturing of volcanic systems: Experimental insights into pre-eruptive conditions, *Earth Planet. Sci. Lett.*, *280*, 211–219, doi:10.1016/j.epsl.2009.01.032.

Tilling, R. I., R. I. Christiansen, W. A. Duffield, E. T. Endo, R. T. Holcomb, R. Y. Koyanagi, D. W. Peterson, and J. D. Unger (1987), The 1972–1974 Mauna Ulu eruption, Kilauea volcano: An example of quasi-steady-state magma transfer, *U.S. Geol. Surv. Prof. Pap.*, *1350*, 405–469.

Tuffen, H., R. Smith, and P. R. Sammonds (2008), Evidence for seismogenic fracture of silicic magma, *Nature*, *453*, 511–514, doi:10.1038/nature06989.

Turcotte, D. L., W. I. Newman, and R. Shcherbakov (2003), Micro and macroscopic models of rock fracture, *Geophys. J. Int.*, *152*, 718–728, doi:10.1046/j.1365-246X.2003.01884.x.

Voight, B. (1988), A method for prediction of volcanic eruptions, *Nature*, *332*, 125–130, doi:10.1038/332125a0.

Voight, B. (1989), A relation to describe rate-dependent material failure, *Science*, *243*, 200–203, doi:10.1126/science.243.4888.200.

Voight, B., and R. R. Cornelius (1991), Prospects for eruption prediction in near real-time, *Nature*, *350*, 695–698, doi:10.1038/350695a0.

Young, H. D. (1992), *Physics*, Addison-Wesley, Reading, U. K.

Zang, A., F. C. Wagner, S. Stanchits, G. Dresen, R. Andresen, and M. A. Haidekker (1998), Source analysis of acoustic emissions in Aue granite cores under symmetric and asymmetric compressive loads, *J. Geophys. Res.*, *135*, 1113–1130.

Zobin, V. M. (2003), *Introduction to Volcanic Seismology*, Elsevier, Amsterdam.

C. Kilburn, Aon Benfield UCL Hazard Centre, Department of Earth Sciences, University College London, Gower Street, London WC1E 6BT, UK. (c.kilburn@ucl.ac.uk)